
Article:
Jeon, S. and Rigby, S.E. (2019) Design and numerical assessment of a rapid-construction corrugated steel-concrete-steel protective structure. International Journal of Protective Structures, 10 (4). pp. 470-485. ISSN: 2041-4196

https://doi.org/10.1177/2041419619830703

Design and Numerical Assessment of a Rapid-Construction Corrugated Steel-Concrete-Steel Protective Structure

S. Jeon & S. E. Rigby*

Department of Civil & Structural Engineering, University of Sheffield, Mappin Street, Sheffield, S1 3JD, UK.

**sam.rigby@shef.ac.uk*

Abstract

A protective structure should be sufficiently resilient to protect its occupants from the harmful effects of an impact or explosion. In many instances, protective structures are also required to be assembled quickly, and be cost-effective. Steel-concrete-steel (SCS) sandwich structures combine the benefits of steel; ductility and anti-scabbing, and concrete; energy absorption and rigidity. Despite these favourable characteristics, the performance of profiled-plate SCS structures under blast and impact loads has yet to be studied in detail. This article presents the results from a numerical study investigating the efficacy of a newly-proposed profiled-plate arched SCS structure under the loading from an extremely near-field high explosive detonation. It is observed that as arch thickness (concrete infill depth) increases, a greater proportion of energy is absorbed through concrete crushing and a larger concrete mass is mobilised. It is shown that a 240 mm arch thickness is adequate to resist the blast load from a 5.76 kg TNT charge, therefore proving the suitability of the proposed protective structure.

Keywords: Blast, Composite, Numerical Analysis, Protective Structure, Steel-Concrete-Steel

1 Introduction

Protective structures should be designed to shield their inhabitants from a range of malicious attacks. One such form of attack, which is the focus of this paper, is the use of high explosive projectiles with the specific intention of causing partial or total collapse of the structure, or damaging the fabric of the structure in a way that compromises its protective ability. Protective structures are common in conflict zones worldwide, and the need for protective structures to be rapidly assembled is often paramount.

The Korean peninsula is a particularly active area of conflict between two neighbour states. In 2010, Yeonpyeong Island was the scene of an artillery engagement between the North Korean military and South Korean forces which resulted in the deaths of up to 15 people and over 50 casualties. In response to this, South Korea began to fortify military facilities and certain civilian shelters using corrugated steel plates as an efficient, cost-effective, and lightweight alternative to reinforced concrete. Numerical and experimental studies have shown the efficacy of earth-covered corrugated steel protective structures (Kim & Lee 2015), however to date there has been no research into corrugated steel protective structures for deployment in situations where construction time is severely constrained.

This paper presents the design of a new type of protective structure designed specifically for rapid construction: a corrugated steel-concrete-steel (SCS) sandwich structure. Numerical analysis is used to

assess the performance of this newly-proposed structure under blast loads and comments are made on the suitability of the proposed design.

2 Literature review

Many blast protection systems exist, each with varying levels of blast resistance and robustness, ease of construction, and cost (Smith 2010). This literature review aims to compile current structural blast protection techniques and evaluate them against these three criteria. The first criterion is commonly evaluated in the literature through numerical and experimental studies, as blast resistance generally has the greatest importance when considering the adequacy of a protective system. Whilst ease of construction and cost are rarely discussed, they are no less significant for real-life systems.

Fibre-reinforced polymer (FRP) sheets have been used to retrofit existing structures to offer increased blast resistance and ductility. Razaqpur et al. (2007) experimentally tested bare reinforced concrete panels and reinforced concrete panels with glass fibre-reinforced polymer (GFRP) sheets adhesively bonded to the front and back faces. The panels were subjected to ANFO charges detonated at scaled distances of 0.9–1.1 m/kg$^{1/3}$, and demonstrated an improved performance when bonded with GFRP sheets. Although more expensive than GFRP, carbon fibre-reinforced polymers (CFRPs) have been shown to demonstrate superior performance (Ronagh & A 2013). Urgessa & Maji (2010) performed a series of blast tests on CFRP retrofitted masonry walls, with the specimens exhibiting considerably less damage as the thickness of the CRFP increased.

Steel fibre-reinforced polymers (SFRPs) are more affordable than CFRPs and have been shown to increase the strength of FRP-wrapped reinforced concrete (RC) columns to a similar extent (Berger et al. 2012), although FRP-wrapped beams are unlikely to demonstrate such an increase in strength owing to the propensity for tensile failure in blast-loaded RC beams (Carriere et al. 2009), as opposed to scabbing or shear failure associated with RC columns. Alternatively, polyurea or polyurethane sprays can be applied directly to a structure to enhance its blast performance (the reader is directed to Raman et al. (2011) for a detailed review). These retrofitting methods, whilst cost-effective and relatively simple to implement, are only suitable for pre-existing structures and are not yet applicable for the design and build of new systems.

Steel-concrete-steel (SCS) sandwich structures combine the benefits of steel; ductility and anti-scabbing, and concrete; energy absorption and rigidity (Liew & Sohel 2009). This construction technique permits high slenderness ratios as the steel layers act as formwork during construction, and the concrete does not require additional reinforcement. Composite action can be achieved through shear connectors which prevent shear failure in the concrete and limit separation of the steel by effectively coupling the deflections of both top and bottom plates (Liew et al. 2017). In order to house these shear connectors, however the SCS panels should be no less than 210 mm thick (Smith 2010), whereas non-composite SCS panels as thin as 50 mm have demonstrated adequate blast resilience against near-field high-explosive blasts (Remennikov & Kong 2012, Wang et al. 2015a). Arched SCS sandwich panels have been shown to displace considerably less than straight SCS panels under dynamic loads: as little as 13% of the residual displacement of straight panels (Liew et al. 2017), and have been suggested for use in diverse applications from blast walls to Arctic caissons to resist the impact load from ice floes (Wang et al. 2016).

Profiled-plate steel sandwich panels are a variation of SCS structures using steel plates formed into different shapes, e.g. sinusoidal or trapezoidal, and are used in various applications owing to their increased resistance against different types of loading when compared to flat plates. To date, there have been few studies which have investigated the performance of profiled-plate SCS structures under blast and impact loads, as identified in the review of Hilo et al. (2015). Despite limited studies into the effectiveness of profiled-plate sandwich structures, there is some evidence to suggest that such systems have increased

cracking resistance and buckling resistance due to confinementoffered by the steel plates (Rafiei et al. 2017). In addition to this, a number of studies demonstrate the effectiveness of using bare profiled steel plates as blast walls, particularly in offshore structures (Malo & Ilstad 1994, Boh et al. 2004, Kim et al. 2014).

Wang et al. (2016) showed that the provision of shear connectors between the steel plates could increase the performance of profiled-plate SCS structures. However, removing the need for shear connectors simplifies the construction and reduces the need for significant pre-fabrication and increased transportation costs. The stackable nature of profiled steel plates also lends itself to efficient transportation. As such, in this paper we neglect composite action and rely only on friction between the concrete and steel, as per Remennikov & Kong (2012), to provide a conservative design solution.

It is posited that un-composite, profiled-plate SCS structures offer a suitable compromise between the strength of a composite SCS structure and the practicality of a flat-plate SCS structure. An arched steel-concrete-steel sandwich structure using corrugated steel plates therefore offers the greatest potential for a rapid-construction protective structure.

3 Design of SCS protective structure

3.1 Design threat

In the military domain, protective structures are subjected to aggressive loads from a number of different sources. Impacts from artillery shells or munitions generate large amounts of kinetic energy and momentum within the structure, however these events are generally considered less significant as protective structures possess sufficient mass to absorb the energy and prevent global deformation or failure. Reinforcing concrete structures with steel plates will significantly improve impact resistance: the hardness of the exterior plate (relative to concrete) will deform or fracture the projectile, reducing its capacity to penetrate the target; and the interior plate (also called the 'backplate') will prohibit scabbing or spalling of the back face of the concrete. Hence, a SCS panel can be expected to have a higher resilience against impact threats when compared to a single sheet of steel or a bare reinforced concrete panel.

Explosions transfer momentum and energy to a target through either direct interaction of blast pressures with the structure (air burst), ground motion and soil impact (below ground explosion), or a combination of the two (surface or near-surface burst). In this study, explosion effects have been identified as the critical case and therefore the proposed SCS structure will be analysed against the effects from bare explosives only, i.e. ground motions will be neglected.

High explosive (HE) projectiles are commonly used in conflicts at the North/South Korean border, and are the focus of this study. HE projectiles are typically loaded with $\sim$15% explosives by mass, and are fitted with either impact, proximity, or timed fuses, or a combination of these. Delayed impact allows the projectile to penetrate some distance into the target before it detonates to increase damage, however these projectiles are expected to deform significantly when impacting a dense, hard material such as steel, or impinging on a profiled surface. As such, penetration is less significant an issue for the proposed design.

In this study, a 152 mm calibre artillery shell with 5.76 kg TNT net explosive quantity was chosen as the design threat (Jeon 2018). The explosive was simplified as an equivalent sphere of TNT (equal mass: 0.095 m radius assuming a density of 1630 kg/m^3) and detonation was assumed to occur shortly after impact. In order to build some degree of conservatism into the model, the centre of mass of the equivalent spherical charge was assumed to be 150 mm from the tip of the shell, as in Figure 1, i.e. the casing is expected to deform and penetrate some distance into the structure whilst the main explosive mass is

expected to remain outside the structure. For simplicity the effects of fragmentation of the explosive casing and the momentum of the shell itself have been neglected in this study.

Figure 1: Geometry of a 152 mm calibre artillery shell (MSM Group 2018) and simplified geometry used in this study

3.2 Structural design specification

Recent research into SCS sandwich structures subjected to extreme loads showed that an arch with a rise-to-span ratio (r/L) of 0.4 was capable of resisting a contact pressure that was ∼170% higher than the failure load of a flat plate ($r/L = 0$) (Huang & Liew 2016). Although higher strength increases were observed for lower rise-to-span ratios, such structures would require larger spans to achieve the same desired internal headroom as an arch with $r/L = 0.4$, and hence a rise-to-span ratio of 0.4 is seen as a suitable compromise between strength increase and economy/practicality, and is selected as the arch geometry to be used in this study. The protective structure is designed to house a 5-ton M-934 military heavy truck. The dimensions of the vehicle and the specified dimensions of the shelter are given in Table 1. Here, 'length', 'height', and 'width' correspond to the y, z, and x axes shown in Figure 2a respectively.

Item	Length (m)	Height (m)	Width (m)	Arch radius (m)	r/L (-)
Vehicle (M-934)	9.271	3.467	2.490	–	–
Protective structure (internal)	9.600	3.750	9.375	4.800	0.4

Table 1: Dimensions of the M-934 vehicle and protective structure

In order to satisfy the requirements of The Republic of Korea Defense Military Facilities Criteria, *Design and Construction Guide for Steel Protective Structures*, DMFC 5-70-80 (ROK Ministry of Defence

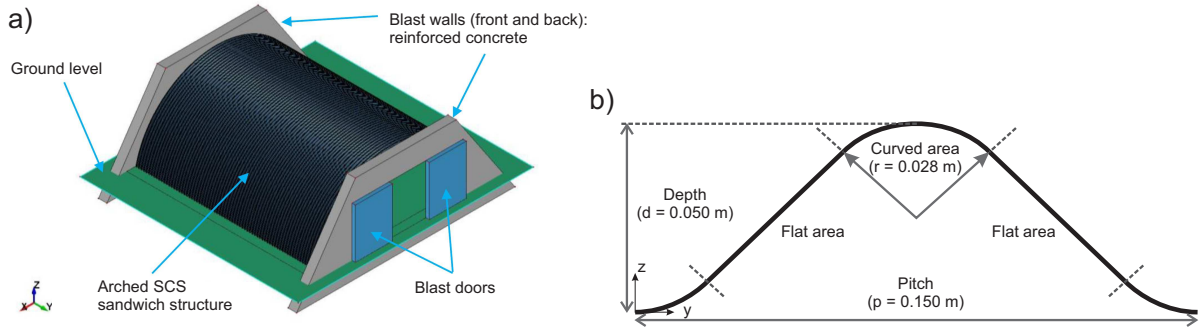

Figure 2: a) Schematic view of the protective structure; b) Profile of corrugated steel plate

2012), standard-depth corrugated steel should posses a yield strength of $\geq$ 245 MPa, an ultimate tensile stress of $\geq$400 MPa, an elongation at failure of $\geq$25%, and an elastic modulus of $\geq$205 GPa. S275 steel possesses suitable properties (275 MPa yield strength, 430 MPa ultimate tensile stress, and 30% elongation at failure) and hence in this study the steel is assumed to be S275 with an elastic modulus of 205 GPa. Standard-depth corrugated steel plates, specified in ROK Ministry of Defence (2012), should have pitch, depth, and curvature radius of 150 mm, 50 mm, and 28 mm respectively (Figure 2b). As thickness can range from 3.65 mm to 7.1 mm, a thickness of 6.32 mm is selected for the plates. DMFC 5-70-80 also specifies the overlapping of plates and bolt connection details. Whilst it is recommended that the structure is *built* in this way, for the purposes of the numerical modelling in this paper the plates have been assumed to act as a single, continuous entity. This is justified with reference to the modelling work of Kim & Lee (2015), Tang et al. (2015), and Ju & Oh (2016).

Since rapid construction is a requirement for the protective structure, it is expected that the structure will be required to be fully functional within 24 hours of construction, hence a high early strength Portland cement should be used for the concrete infill. According to the Korean Standard, *Portland Cement*, KS L-5201 (KATS 2016), high early-strength Portland cement falls into Category 3, and it must have a compressive strength of 10 MPa or higher after 24 hours. Furthermore, the concrete should possess a characteristic strength, $f_{ck} \geq 18$ MPa (ROK Ministry of Defence 2012). After a review of available commercial products, the concrete has been assumed to possess a characteristic strength at 24 hours of 22.2 MPa and an elastic modulus of 27.3 GPa (Jeon 2018). Coarse aggregates were assumed to have a maximum size of $<$ 19 mm.

For simplicity, it has been assumed that reinforced concrete footings provide adequate lateral and rotational restraint at the supports such that the SCS structure can be assumed to be perfectly clamped.

4 Numerical modelling setup

4.1 Geometric representation

Numerical models were simulated using the LS-DYNA explicit solver, LSDYNA V971 R8.10, (Hallquist 2006). The corrugated steel plates were represented using Belytschko-Tsay elements with two through-thickness integration points and appropriate controls to prevent hourglassing. For the concrete infill, constant-stress solid elements were chosen to better model complex behaviour and material failure in mechanisms such as scabbing and spalling.

A comprehensive mesh sensitivity analysis was performed as part of a preliminary modelling study in Jeon (2018). Whilst detailed results are omitted here for brevity, the models analysed in this paper were designed in accordance with the following findings:

- The corrugated plates were created using line elements, connecting three keypoints per flat part and three keypoints per curved part of the plate, to match the profile in Figure 2b). An individual line segment (pitch 150 mm), comprising these keypoints, was copied to cover the length of the structure and then extruded into the arch shape (note the coordinate axes in Figure 2)
- The converged element size for the corrugated steel plates was found to be 0.06 m, and the converged element size for the concrete infill was found to be 0.04 m
- The centreline of the structure, in the direction parallel to the span of the arch, was specified as a symmetry boundary (see Figure 3). The charge was assumed to load the protective structure at some point along this symmetry line, with the exact impact locations to be defined later in this manuscript
- Preliminary findings indicated that it was not necessary to model the full length of the structure (where 'length' refers to the distance perpendicular to the span, as per Figure 3). Deformation histories for a 3.6 m structural length (1.8 m in half-symmetry) were found to closely match deformation histories for a full-length 9.6 m structure (4.8 m in half-symmetry). This is justified by the highly localised nature of the imparted loading and resultant structural deformation. The end of the structure remote from the symmetry plane was modelled as a free boundary as negligible deformations were expected

4.2 Material properties

The steel was represented as a bilinear elastic-plastic material using the *MAT_PLASTIC_KINEMATIC material model with density 7850 kg/m^3, elastic modulus 205 GPa, static yield strength $\sigma_0 = 275$ MPa, tangent modulus 1 GPa, and failure strain of 0.3, after Remennikov & Kong (2012). Dynamic yield strength, σ_d, was scaled using the Cowper-Symonds strain-rate sensitivity law (Cowper & Symonds 1957):

$$\sigma_d = \sigma_0 \left[1 + \frac{\dot{\epsilon}}{C}^{\frac{1}{p}} \right] \tag{1}$$

where $\dot{\epsilon}$ is uniaxial plastic strain-rate, and C and p are material constants, which were set at 40.4 and 5.0 respectively, after Wang et al. (2015b).

The concrete was modelled using the 'continuous surface cap model', *MAT_CSCM_CONCRETE, an elasto-plastic damage model with rate effects which is particularly suited for simulating dynamic events for concrete with compressive strength between 20–58 MPa and coarse aggregate sized between 8–32 mm (Murray 2007). The concrete will exhibit strain hardening until the stress level reaches the yield failure surface, which is given as a combination of the shear failure surface and hardening compaction surface (cap). After this point, the concrete begins softening, based on either brittle damage (tension) or ductile damage (compression). In this study, both forms of damage were permitted and the maximum of either type was taken as the damage level. In line with the requirements outlined in the design specification previously, a compressive strength of 22.2 MPa and aggregate size of 19 mm was used in this study. The concrete was modelled with a density of 2350 kg/m^3.

*MAT_CSCM_CONCRETE also allows for element erosion, i.e. the deletion of elements which have reached the maximum allowable principal strain. These elements are then excluded from subsequent computations. Whilst erosion may allow for a more accurate description of material failure, it is important to

note that it may yield unrealistic behaviour if the element size is much larger than the actual size of the cement and aggregates. Remennikov & Kong (2012) argue that the use of element erosion can lead to a significant underestimation of the overall capacity of concrete, which was supported by numerical results for models without erosion that compared better with experimental data than the results from models with erosion included. Jeon (2018) found that the internal energy of the concrete infill was significantly under-predicted if the elements were allowed to erode. Element erosion is therefore prohibited in this study, however plastic failure of concrete can still be reported, even if those elements are not eroded.

4.3 Loading, boundary conditions, and contact

Loading was applied to the structure using the *LOAD_BLAST_ENHANCED (LBE) subroutine in LS-DYNA, after Randers-Pehrson & Bannister (1997). LBE applies the Kingery & Bulmash (1984) semi-empirical pressure-time predictions directly to the element surface normals, with the following trigonometric correction for angle of incidence effects:

$$p(t, \alpha) = p_r(t) \cos^2 \alpha + p_{so}(t) \left[1 + \cos^2 \alpha - 2 \cos \alpha\right]. \tag{2}$$

where p is the pressure applied to the element, t is time, α is angle of incidence, defined as the angle between the surface normal and a line from the centre of the explosive to the element centroid (Rigby et al. 2015a), and p_r and p_{so} are the normally reflected ($\alpha = 0°$) and incident ($\alpha = 90°$) pressures respectively at the element centroid.

Recent numerical (Shin et al. 2015) and experimental work (Rigby et al. 2015b) has shown that the Kingery & Bulmash (1984) predictions, particularly for reflected specific impulse, remain reasonably accurate at distances extremely close to an explosive charge. Applying the load directly to the structure removes the need to model a fluid domain surrounding the structure and associated, computationally expensive, fluid-structure interaction.

The structure was modelled using half-symmetry by assigning appropriate boundary conditions (constrained y displacements and x, and z rotations) on a line of symmetry along the span of the arch. Thus, only 1.8 m length was required to model a representative length of the entire structure, see Figure 3. As the DMFC 5-70-80 (ROK Ministry of Defence 2012) specifies perfectly clamped supports, the parts of the structure that sit below ground level (a height of 1.05 m from the bottom of the arch) were constrained against all degrees-of-freedom.

Coupling between the steel plates and concrete infill was achieved using the *CONTACT_AUTOMATIC_SURFACE_TO_SURFACE keyword in LS-DYNA with default stiffness factors and a coefficient of friction of 0.2 (Remennikov & Kong 2012). A small offset was specified between the steel and concrete parts (1E-6 m), and an automatic correction routine was run prior to solving the models to remove any areas where the steel and concrete meshes had overlapped. This was achieved by adjusting the positions of any nodes that had overlapped, and ensures that artificial disturbances caused by spurious contact do not propagate into the mesh and corrupt the results.

4.4 Situations studied

Five different models were run. Firstly, a 120 mm thick arch was analysed under three different blast loads: 1, a 5.76 kg spherical TNT charge, detonated as a free air burst at 150 mm stand-off (to-centre) directly above the top-centre of the arch; 2, a 5.76 kg spherical TNT charge, detonated as a free air burst at 150 mm stand-off (to-centre), half-way between the ground surface and the top of the arch; 3, a 5.76 kg hemispherical TNT charge detonated on the surface, 150 mm stand-off (to-centre) from the base of the arch. These are labelled 'Near-field 1–3' in Figure 4, and θ refers to the angle between the explosive and

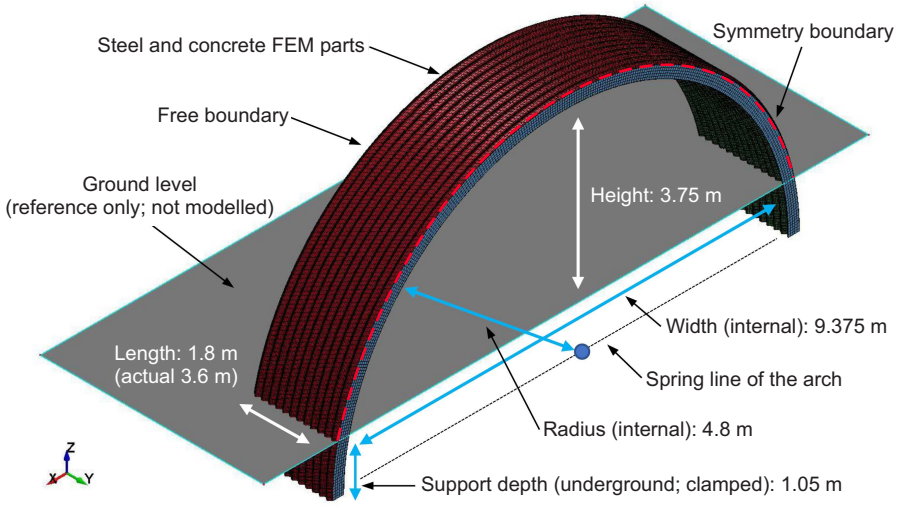

Figure 3: Geometry and dimensions of the numerical model

the centre of the spring line of the arch (note: this is different to the angle of incidence, α which is a function of the orientation of the arch and the profile of the steel plate, as well as the relative position of the explosive). All charges were placed on the symmetry plane and therefore only half of the structure was modelled.

An additional verification case was studied: that of a 5.76 kg hemispherical TNT charge detonated on the surface, 1800 mm stand-off (to-centre) from the base of the arch ('Far-field' in Figure 4), however the results are omitted in this article as the structure remained elastic throughout and displacements were negligible. Once the worst-case loading scenario was identified from 'Near-field 1–3' for the 120 mm arch thickness, two further models were run with this loading condition applied to 180 mm and 240 mm arch thicknesses. The steel plate thickness was kept constant at 6.32 mm throughout.

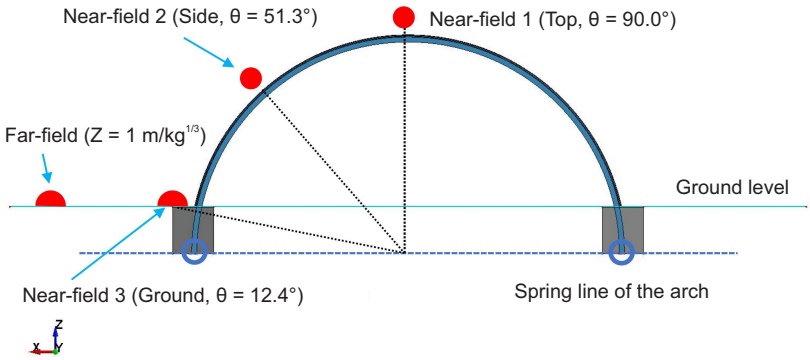

Figure 4: Loading arrangements studied in this article

Figure 5 shows the magnitude and distribution of reflected pressure distributions on the roof of the protective structure (in plan view) at various instants in time. Here, the bottom edge of the structure acts as the symmetry boundary and hence the loading is symmetric above and below this line (as per the dashed line in Figure 5a). It should be noted that whilst the fringe levels are clipped at a reflected pressure of 100 MPa, the peak reflected pressure directly beneath the charge reaches a value of ∼400 MPa. However, this pressure is highly localised and decays rapidly with both space and time. It can be seen that areas of the corrugated plate orientated towards the charge are subjected to a higher load, and those orientated away from the charge are subjected to a lower load owing to angle of incidence effects.

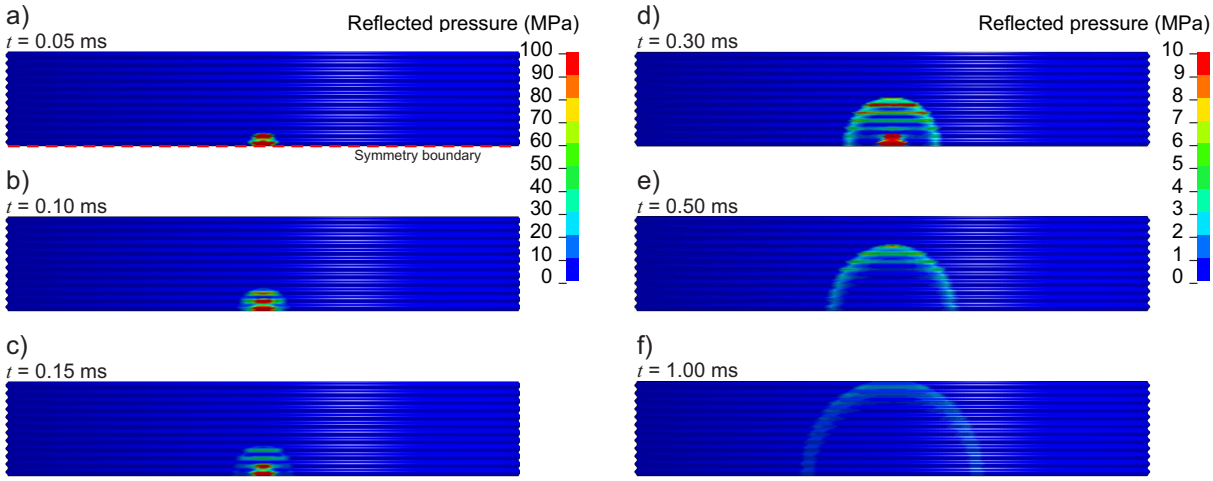

Figure 5: Pressure contours acting on the roof of the protective structure for Near-field 1 loading condition

5 Assessment of SCS protective structure

5.1 Identification of worst-case loading scenario

The initial models were run for 30 ms under all three loading conditions, with the displacement-time history of the node located directly beneath the charge shown in Figure 6a. Additionally, the separation distance between the steel backplate and the concrete infill was calculated and is plotted in Figure 6b.

Whilst the charge in Near-field 3 experiences an amplification from the ground surface[1], the resultant displacement is still considerably less than the displacements under Near-field 1 and 2. Provided the structure's foundations are adequate to provide lateral and rotational restraint, the structure possesses sufficient shear resistance to resist this load.

Both the peak displacement and maximum backplate-concrete separation distance are greatest for Near-field 2. It is suggested that the (primarily) vertical loading imparted from Near-field 1 allows the structure to better contain the compressive thrust due to its arched shape, whereas in Near-field 2 a significant amount of lateral load is imparted, which results in greater displacement and separation.

[1] i.e. it has been modelled as a hemispherical surface burst rather than a spherical free-air burst, with an effective mass increase factor of 1.8, after Kingery & Bulmash (1984)

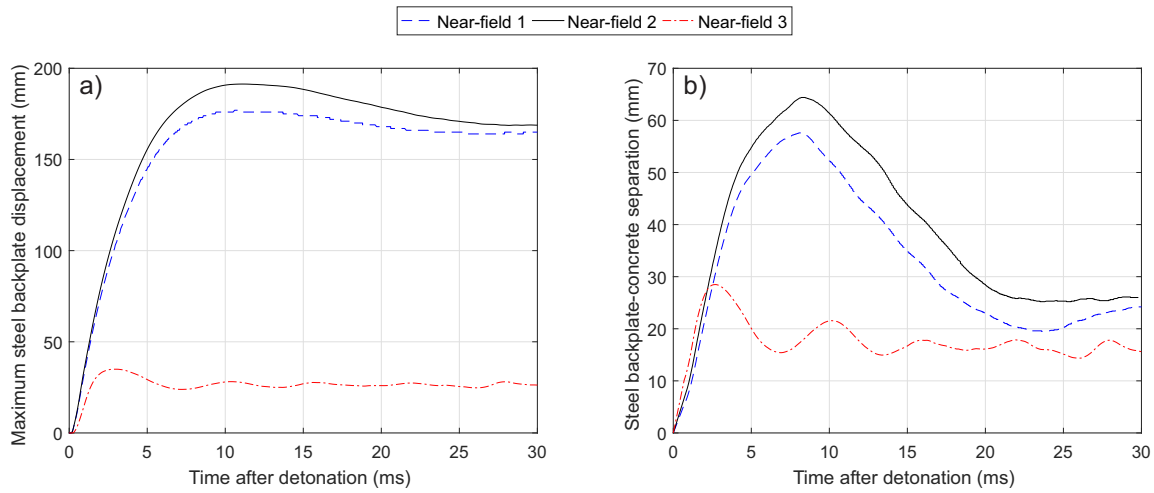

Figure 6: Numerical results from worst-case loading study: a) Maximum resultant displacement in the steel backplate; b) Separation distance between concrete infill and steel backplate

Figure 7 shows fringe plots of resultant displacement of the steel backplate and effective plastic strain in the concrete infill, for Near-field 1–3 load cases. The deformation in the steel plate is highly localised and the deformation and concrete damage at the edge of the structure remote from the charge is effectively zero,justifying the assumption that a structural length of 3.6 m is adequate to describe the response of the entire structure. Despite the high-magnitude loading, the steel does not reach its failure strain and therefore in all cases the interior of the structure is not breached. In Near-field 1 and 2 there is a region of pulverised concrete close to the location of the charge, which is retained by the steel backplate. The percentage of concrete that has failed, by volume, is 7.8% and 7.4% in Near-field 1 and 2 respectively. On account of the larger structural displacements and similar concrete failure, Near-field 2 is selected as the worst-case loading scenario.

5.2 Effect of arch thickness

Two additional arch thicknesses were analysed under the Near-field 2 loading arrangement: 180, and 240 mm, and are compared against the results for the 120 mm thick arch. Analyses were run for 90 ms to allow for a more complete description of structural response. Figure 8a shows displacement-time histories of the nodes located directly beneath the charge for each arch thickness, and Figure 8b shows the separation distance between the steel backplate and the concrete infill for each arch thickness.

As expected, an increase in concrete infill results in a significant increase in stiffness and therefore a decrease in peak displacement. The maximum values of displacement are 192 mm, 80 mm, and 52 mm for the 120 mm thick, 180 mm thick, and 240 mm thick arches respectively. It is interesting to note that, whilst a thicker arch demonstrates a stiffer response to the imparted blast load, there is not as pronounced a benefit on backplate-concrete separation distance (Figure 8b). The maximum separation distances are 64 mm, 16 mm, and 13 mm for the 120 mm thick, 180 mm thick, and 240 mm thick arches respectively. Interestingly, the residual separation distance for the 240 mm arch is 11 mm, which is greater than the residual separation distance of 9 mm for the 180 mm arch.

The deformed profiles of the 180 mm thick and 240 mm thick arches differ from the profile of the

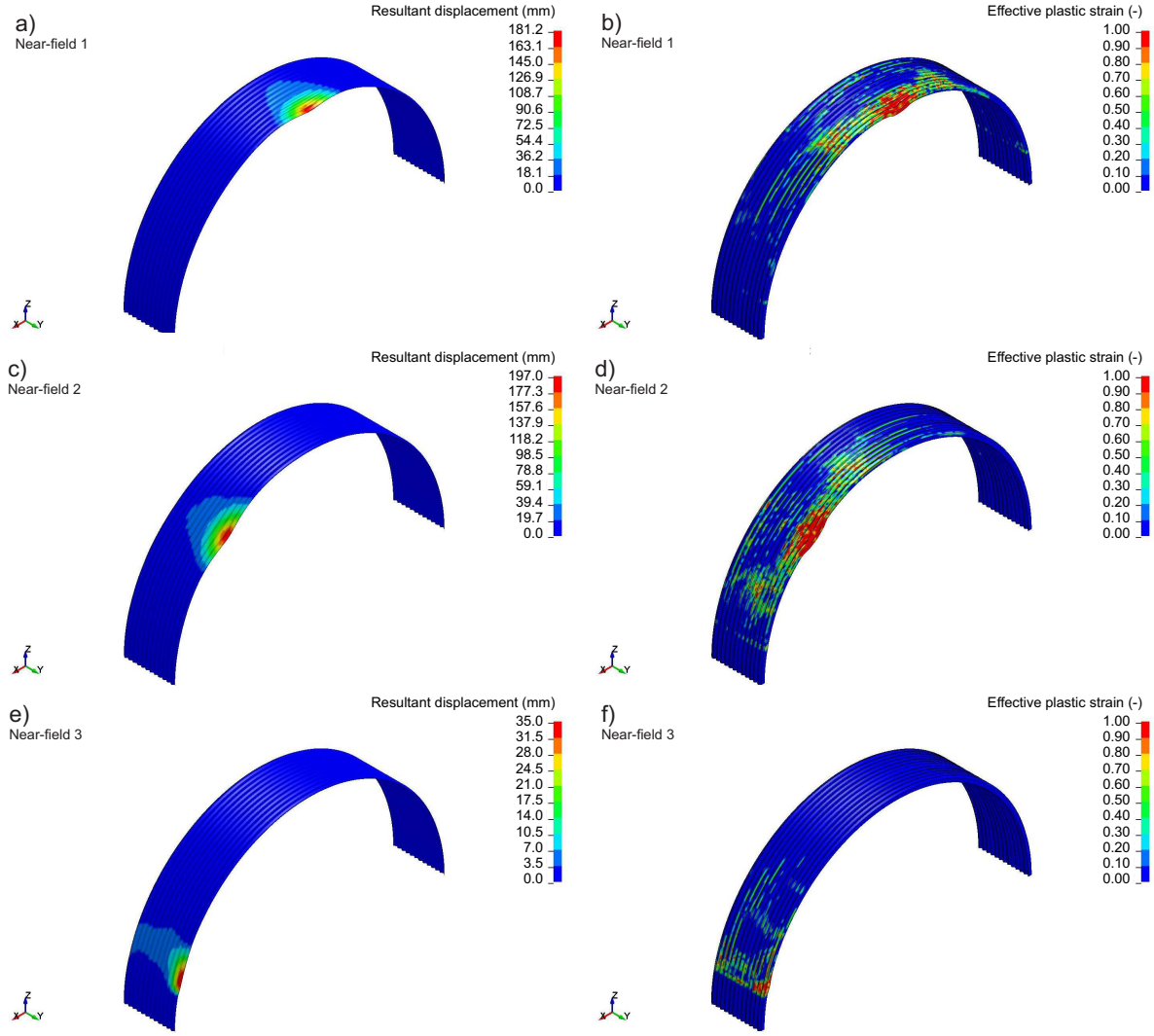

Figure 7: Fringe plots of maximum resultant displacement in the steel backplate (a, c, e) and effective plastic strain in the concrete (b, d, f) for Near-field 1–3 load cases, 120 mm arch thickness

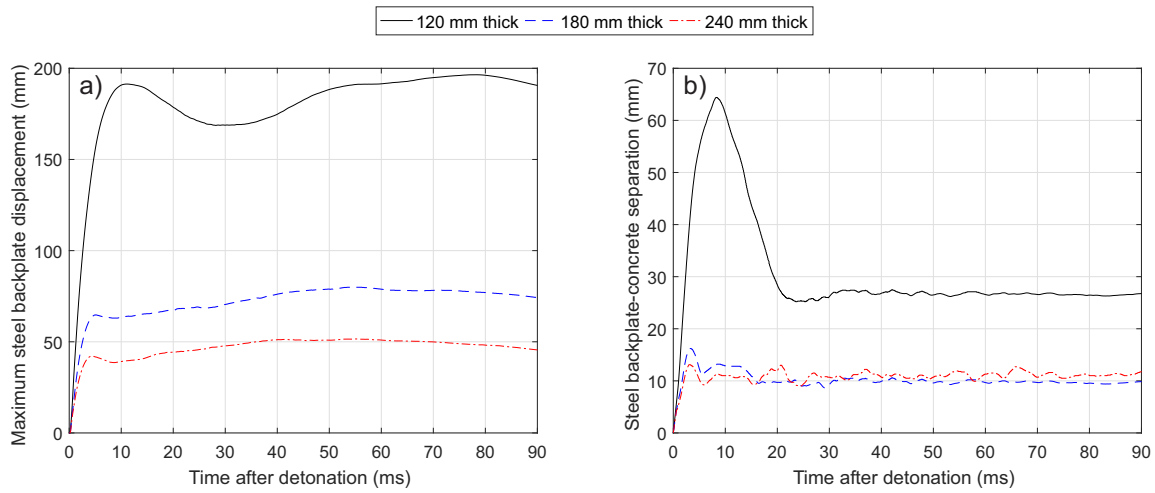

Figure 8: Numerical results from arch thickness study: a) Maximum resultant displacement in the steel backplate; b) Separation distance between concrete infill and steel backplate

120 mm thick arch, as can be seen in the fringe plots of resultant displacement of the steel backplate and effective plastic strain in the concrete infill in Figure 9. As thickness increases, deformation in the steel backplate becomes lower in magnitude but is spread over a larger area. The concrete failure is also less localised, as more of the concrete mass is mobilised to resist the imparted load. 7.2% of the concrete infill in the 180 mm arch fails (1680 kg, by mass), whereas 7.7% of the concrete in the 240 mm arch fails (2320 kg, by mass).

Table 2 shows the energy absorbed in each part for the different arch thicknesses studied. This confirms the observations that as arch thickness increases, a greater proportion of concrete is mobilised, and the work done by the steel backplate begins to increase with increasing thickness (beyond a certain value between 180 and 240 mm). This also explains why an increase in residual backplate-concrete separation was seen for the 240 mm thick arch (Figure 8b). The energy absorbed in the concrete layer is approaching the value of 50% as observed in Wang et al. (2016).

Arch thickness (mm)	Energy absorbed by each part (%)		
	Exterior steel plate	Concrete infill	Interior steel plate ('back-plate')
120	61	26	13
180	59	34	7
240	55	37	8

Table 2: Energy absorbed in each part for different arch thicknesses

There appears to be a trade-off between increased stiffness of a thicker arch, and the corresponding increase in the mass of mobilised concrete and therefore greater requirements for the steel backplate to resist the inertia of the concrete as it spalls. Whilst both 180 mm and 240 mm arch thicknesses appear

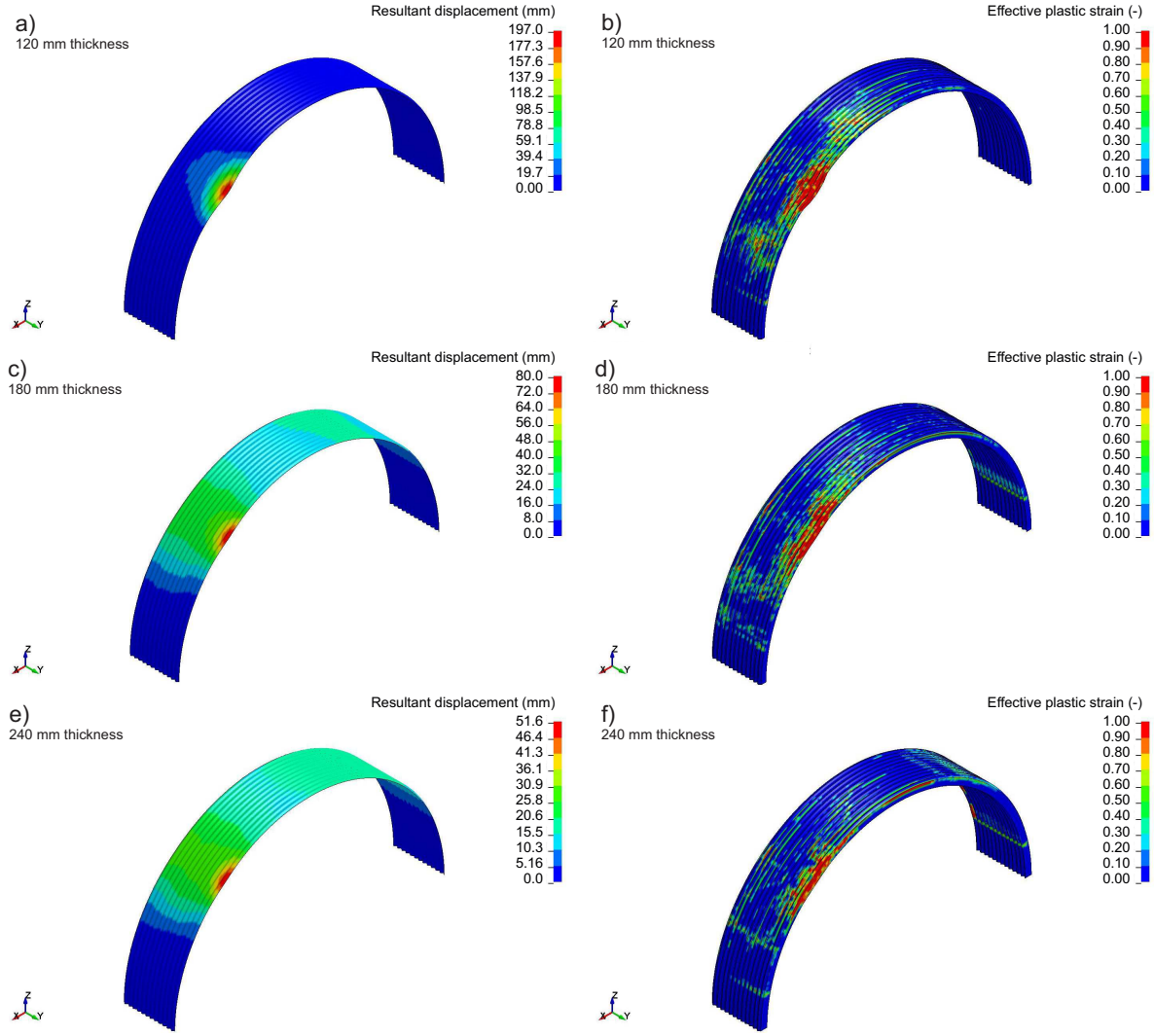

Figure 9: Fringe plots of maximum resultant displacement in the steel backplate (a, c, e) and effective plastic strain in the concrete (b, d, f) for 120–240 m arch thickness, Near-field 2 loading

to offer a suitable balance of these properties, it is suggested that: a) thicknesses below 180 mm do not possess sufficient stiffness, and; b) there may be a critical thickness above 240 mm where the inertia of the failed concrete cannot be resisted by the steel backplate and therefore the structure is breached. The optimal arch thickness is therefore within the range of 180–240 mm.

5.3 Recommendations

DMFC 5-70-80 (ROK Ministry of Defence 2012) provides limits on the allowable ductility ratio (peak displacement divided by elastic deflection limit) of a protective structure, namely this value is not allowed to exceed 1.75 if tensile membrane action is prohibited, or 6.00 if tensile membrane action is allowed. These ratios were found to be approximately equal to displacements of 16.0 mm and 54.0 mm respectively for the structures analysed in this article. It was found that there was little sensitivity on this value for the different thicknesses of concrete infill, as the failure was primarily driven by deformation of the steel backplate which was the same thickness throughout.

Of the three arches studied, only the 240 mm thick arch meets this criteria (peak displacement of 52 mm $<$ 54 mm). It can be said that, under a *direct hit* from the design threat (152 mm calibre artillery shell with 5.76 kg TNT net explosive quantity), a 240 mm thick arched profiled-plate SCS sandwich structure is *conditionally safe*, provided adequate tensile membrane resistance is provided by the steel backplate as it is deforming. This can be achieved through following guidance in DMFC 5-70-80 with regards to the overlapping of plates and bolt connection details. Whilst an increase in structural mass may be detrimental for earthquake resistance, the risk to this protective structure from an explosive attack is significantly greater, and hence an increase in arch thickness is largely beneficial.

Although none of the structures failed by breaching, both the 120 mm and 180 mm thick arches do not meet the criteria set in DMFC 5-70-80 (peak displacements of 192 mm and 80 mm respectively), and do not offer adequate protection under the design threat. It was found, however, that all structures provided adequate resistance against the 'Far-field' loading condition (Figure 4), and therefore a structure of 120 mm arch thickness provides adequate resistance against an *indirect hit* from the design threat.

6 Summary and conclusions

A review of the available literature identified a lack of studies investigating the performance of profiled-plate steel-concrete-steel protective structures. Such structures have the potential to be robust, simple to construct, and cost-effective. This article presents the results from a numerical study on the efficacy of profiled-plate arched steel-concrete-steel sandwich structures using LS-DYNA (Hallquist 2006). The structure is designed to house a M-934 military heavy truck, and has an internal width of 9.375 m, height of 3.750 m, and length of 9.600 m. Steel and concrete properties and fabrication techniques are assumed to be in accordance with design guidance. Three different arch thicknesses are studied: 120 mm, 180 mm, and 240 mm. 6.32 mm thick corrugated steel plates were used throughout.

A design threat is specified, namely a 152 mm calibre artillery shell (5.76 kg TNT NEQ) detonated shortly after contact with the structure. The charge is modelled as an equivalent mass sphere with its centre located 150 mm from the surface of the protective structure. Loading is applied to the structure using the in-built *LOAD_BLAST_ENHANCED subroutine, which directly maps Kingery & Bulmash (1984) pressure predictions as load curves. A preliminary study indicated that a charge detonated 1/4 along the length of the arch represented the worst-case scenario.

It was observed that a considerable amount of concrete was pulverised by the blast load in the area close to the charge, but scabbing/spalling of the concrete was succesfully contained by the steel backplate for all structures analysed. The amount of failed concrete was seen to increase with increasing arch

thickness as a greater proportion of the total energy was absorbed through concrete crushing. Accordingly, residual detachment between the concrete and steel backplate was also seen to increase when the arch thickness increased from 180 mm to 240 mm.

Of the structures studied in this paper, it is concluded that a 240 mm arch, fabricated to standards specified in DMFC 5-70-80 (ROK Ministry of Defence 2012) to allow for tensile membrane action in the steel backplate, provides adequate resistance against the design threat. This article therefore demonstrates the suitability of an arched SCS sandwich structure using profiled steel plate as a rapid-construction protective structure, which demonstrates favourable characteristics, namely: spalling/scabbing resistance; increased cracking and buckling resistance; and hardness/ductility from the profiled steel plates. The proposed structure is easier to assemble and more cost-effective than equivalent earth-covered structures currently in use.

References

Berger, J., Heffernan, P. & Wight, R. (2012), 'Blast testing of CFRP and SRP strengthened RC columns', *WIT Transactions on State of the Art in Science and Engineering* **60**, 189–198.

Boh, J., Louca, L. & Choo, Y. (2004), 'Strain rate effects on the response of stainless steel corrugated firewalls subjected to hydrocarbon explosions', *Journal of Constructional Steel Research* **60**(1), 1–29.

Carriere, M., Heffernan, P., Wight, R. & Braimah, A. (2009), 'Behaviour of steel reinforced polymer (SRP) strengthened RC members under blast load', *Canadian Journal of Civil Engineering* **36**(8), 1356–1365.

Cowper, G. & Symonds, P. (1957), Strain-hardening and strain-rate effects in the impact loading of cantilever beams, Technical Report 28, Division of Applied Mathematics, Brown University, Providence, RI, USA.

Hallquist, J. O. (2006), *LS-DYNA Theory Manual*, Livermore Software Technology Corporation, CA, USA.

Hilo, S., Wan Badaruzzaman, W., Osman, S., Al-Zand, A., Samir, M. & Hasan, Q. (2015), 'A state-of-the-art review on double-skinned composite wall systems', *Thin-Walled Structures* **97**, 74–100.

Huang, Z. & Liew, J. (2016), 'Steel-concrete-steel sandwich composite structures subjected to extreme loads', *International Journal of Steel Structures* **16**(4), 1009–1028.

Jeon, S. (2018), *A Design Proposal of a Rapid-Construction Protective Structure Using Corrugated Steel-Concrete Sandwich Structure*, MSc Dissertation, Department of Civil and Structural Engineering, University of Sheffield, United Kingdom.

Ju, M. & Oh, H. (2016), 'Static and fatigue performance of the bolt-connected structural jointed of deep corrugated steel plate member', *Advances in Structural Engineering* **19**(9), 1435–1445.

KATS (2016), *Portland Cement*, Korea Agency for Technology and Standards (KATS), KS L-5201.

Kim, S. & Lee, J. (2015), 'Blast resistant performance of bolt connections in the earth covered steel magazine', *International Journal of Steel Structures* **15**(2), 507–514.

Kim, S., Sohn, J., Lee, J., Li, C., Seong, D. & Paik, J. (2014), 'Dynamic structural response characteristics of stiffened blast wall under explosion loads', *Journal of the Society of Naval Architects of Korea* **51**(5), 380–387.

Kingery, C. N. & Bulmash, G. (1984), Airblast parameters from TNT spherical air burst and hemispherical surface burst, Technical Report ARBRL-TR-02555, U.S Army BRL, Aberdeen Proving Ground, MD, USA.

Liew, J. & Sohel, K. (2009), 'Lightweight steel-concrete-steel sandwich system with J-hook connectors', *Engineering Structures* **31**(5), 1166–1178.

Liew, J., Yan, J. & Huang, Z. (2017), 'Steel-concrete-steel sandwich composite structures – Recent innovations', *Journal of Constructional Steel Research* **130**, 202–221.

Malo, K. & Ilstad, H. (1994), 'Response of corrugated steel walls due to pressure loads', *Structures under Shock and Impact* **8**, 165–173.

MSM Group (2018), '152 mm ammunition', https://www.msm.sk/en/msm-group/zvs/ammunition/medium-and-big-caliber-ammunition/152-mm-ammunition/. Last accessed: 05-09-2018.

Murray, Y. (2007), Users manual for LS-DYNA concrete material model 159, Technical Report FHWA-HRT-05-062, US Department of Transportation, Federal Highway Administration, McLean, VA, USA.

Rafiei, S., Hossain, K., Lachemi, M. & Behdinan, K. (2017), 'Impact shear resistance of double skin profiled composite wall', *Engineering Structures* **140**, 267–285.

Raman, S., Ngo, T. & Mendis, P. (2011), 'A review on the use of polymeric coatings for retrofitting of structural elements against blast effects', *Electronic Journal of Structural Engineering* **11**, 69–80.

Randers-Pehrson, G. & Bannister, K. (1997), Airblast loading model for DYNA2D and DYNA3D, Technical Report ARL-TR-1310, U.S Army Research Laboratory, Aberdeen Proving Ground, MD, USA.

Razaqpur, G., Tolba, A. & Contestabile, E. (2007), 'Blast loading response of reinforced concrete panels reinforced with externally bonded GFRP laminates', *Composites Part B: Engineering* **38**(5), 535–546.

Remennikov, A. & Kong, S. (2012), 'Numerical simulation and validation of impact response of axially-restrained steelconcretesteel sandwich panels', *Composite Structures* **94**(12), 3546–3555.

Rigby, S., Fay, S., Tyas, A., Warren, J. & Clarke, S. (2015a), 'Angle of incidence effects on far-field positive and negative phase blast parameters', *International Journal of Protective Structures* **6**(1), 23–42.

Rigby, S. et al. (2015b), 'Observations from preliminary experiments on spatial and temporal pressure measurements from near-field free air explosions', *International Journal of Protective Structures* **6**(2), 175–190.

ROK Ministry of Defence (2012), *Design and Construction Guide for Steel Protective Structures*, Defense Military Facilities Criteria, DMFC 5-70-80.

Ronagh, H. & A, E. (2013), 'Flexural retrofitting of RC buildings using GFRP/CFRP – A comparative study', *Composites Part B: Engineering* **46**, 188–196.

Shin, J., Whittaker, A. & Cormie, D. (2015), 'Incident and Normally Reflected Overpressure and Impulse for Detonations of Spherical High Explosives in Free Air', *Journal of Structural Engineering* **04015057**(13), 1–13.

Smith, P. (2010), 'Blast walls for structural protection against high explosive threats: A review', *International Journal of Protective Structures* **1**(1), 67–84.

Tang, G., Yin, L., Guo, X. & Cui, J. (2015), 'Finite element analysis and experimental research on mechanical performance of bolt connections of corrugated steel plates', *International Journal of Steel Structures* **15**(1), 193–204.

Urgessa, G. & Maji, A. (2010), 'Dynamic response of retrofitted masonry walls for blast loading', *Journal of Engineering Mechanics* **136**(7), 858–864.

Wang, Y., Liew, J. & Lee, S. (2015a), 'Experimental and numerical studies of non-composite steel-concrete-steel sandwich panels under impulsive loading', *Materials and Design* **81**, 104–112.

Wang, Y., Liew, J. & Lee, S. (2015b), 'Theoretical models for axially restrained steel-concrete-steel sandwich panels under blast loading', *International Journal of Impact Engineering* **76**, 221–231.

Wang, Y., Zhai, X., Lee, S. & Wang, W. (2016), 'Responses of curved steel-concrete-steel sandwich shells subjected to blast loading', *Thin-Walled Structures* **108**, 185–192.